Parton Cascade Evolution and Event Structure at HERA

M. Bengtsson[a], G. Ingelman[b], T. Sjöstrand[c]

[a] Institut für Theoretische Physik, RWTH, D-5100 Aachen, FRG
[b] Deutsches Elektronen-Synchrotron DESY, Notkestrasse 85, D-2000 Hamburg 52, FRG
[c] Department of Theoretical Physics, University of Lund, Sölvegatan 14A, S-223 62 Lund, Sweden

Abstract

Perturbative QCD corrections to leptoproduction events can be introduced either in the form of matrix elements or of parton showers. Each of these approaches has its advantages and disadvantages, making a comparison of the two interesting. In this paper, a model for parton shower evolution in leptoproduction is outlined. The influence of QCD effects on the expected event structure at HERA is investigated in detail. This includes multiplicity and momentum distributions, transverse momentum flow and correlations, as well as jet properties.

1 Introduction

Leptoproduction is one of the main fields of experimental high energy physics, with a program complementary to the ones offered by e^+e^- annihilation and hadron collisions. Studies at higher energies have two main objectives, to improve current understanding of the standard model and to look for signals for new physics. At HERA, these studies will be based both on the overall kinematical variables and on the detailed event structure.

The two main kinematical variables, x and Q^2, can be calculated from a knowledge of incoming and scattered lepton momenta. At HERA, this procedure is straightforward in neutral current (γ/Z^0 exchange) events, but less so in charged current ($W^\pm$ exchange) ones, where the outgoing neutrino is not detected. If the hadronic system in the event can be measured, energy-momentum conservation gives the neutrino momentum, however. It then becomes a matter of understanding the detailed response of a detector, in particular degradations due to an imperfect angular coverage, which presupposes a knowledge of the structure of the hadronic system. Some of this knowledge, but not all, may come from a 'calibration' in neutral current events, where both the scattered electron and the hadronic system may be observed. Also a more elaborate study of the event shape, e.g. a search for new particles decaying into several jets, or combinations of leptons and jets, must be based on some notion of what to expect from standard model backgrounds. Hence, it is important to have as well-founded expectations as possible for the event structure in high energy leptoproduction.

The required understanding of hadron production is today not provided directly by QCD. Rather, a composite picture is used, wherein a perturbative treatment of parton production is combined with a nonperturbative model for the fragmentation of a partonic state into hadrons. In the latter capacity, the Lund string model [1] will be used throughout. For the perturbative part, two main alternatives are possible: matrix elements and parton showers. In principle, the former approach is superior, in that matrix elements involve no kinematical approximations and in that the complete structure in x and Q^2 is included. For fixed target energies, the matrix element route has already been proven phenomenologically viable [2,3,4]. However, experience with experiments at PETRA and PEP have taught us that not even second order matrix elements provide a satisfactory description of data at or above $W = 30$ GeV [5]. In particular, the amount of multijet events is underestimated, indicating a need for higher order corrections. It is therefore not to be expected that the matrix elements at our disposal in leptoproduction, which are of first rather than second order, should fare any better at the larger W-values probed with HERA. Parton showers are based on an iterative picture of successive branchings. Multiparton configurations are therefore generated in a natural fashion, resulting in an improved agreement with the multijet phenomenology in e^+e^- annihilation [5]. The parton shower approach should therefore also give a more realistic picture of the complexity of high energy leptoproduction events than that offered by first order matrix elements. Unfortunately, the parton shower algorithms include various kinematical simplifications, making the results particularly uncertain for the amount of hard emission.

In a previous paper [6], one specific model for parton shower evolution is developed. In a second paper [7], results at fixed target energies, HERA and LEP+LHC energies are presented, with a comparison of parton shower and matrix element predictions. The current report represents a synthesis of these two papers, where material relevant for HERA studies have been collected. In section 2 is given a brief introduction to the simple quark parton model (QPM), without any QCD corrections, and its matrix element (ME) and parton shower (PS) extensions. Predictions for HERA energies, with a comparison between the three alternatives above, are found in section 3. A summary and outlook is given in section 4. Further details, in particular on comparisons with fixed target data, may be found in the original papers [6,7]. Some QCD studies are also found in these papers and for a more detailed investigation of QCD tests possible at HERA we refer to [8].

2 The Models

2.1 The Quark Parton Model

The kinematics of leptoproduction, Fig. 1, is given in terms of the four-momenta k and k' of the incoming and outgoing lepton and the nucleon target momentum vector P. The momentum of the exchanged electroweak current, $q = k - k'$, is a spacelike vector, i.e. $q^2 = -Q^2$, $Q^2 > 0$. A commonly used variable is ν, defined by the relation $m_p\nu = P \cdot q$, i.e. the energy of the current in the target rest frame. The scaling variables are given by

$$x \equiv \frac{Q^2}{2P \cdot q} = \frac{Q^2}{2m_p\nu} \tag{1}$$

$$y \equiv \frac{P \cdot q}{P \cdot k} = \frac{2P \cdot q}{s} = \frac{\nu}{\nu_{max}} \tag{2}$$

where $s = (P + k)^2$ is the total invariant mass-squared. The invariant mass of the hadronic final state, which is an important variable both for perturbative QCD and hadronization, is given by

$$W^2 \equiv (P + q)^2 = Q^2 \frac{1 - x}{x} + m_p^2 \tag{3}$$

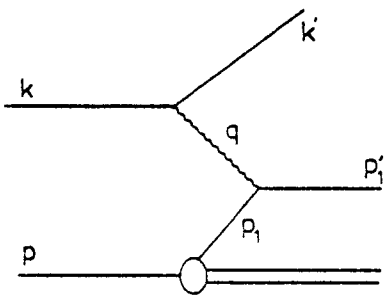

Figure 1: *Kinematics notation for the naive parton model, i.e. without any QCD corrections. Particles that appear 'after' the boson exchange are denoted with a prime. The proton four-momentum is denoted by capital P.*

The deep inelastic scattering cross-section can be well illustrated by that of the purely electromagnetic interaction, i.e. photon exchange,

$$\frac{d^2\sigma}{dx\,dQ^2} = \frac{2\pi\alpha^2}{xQ^4}\{1+(1-y)^2\}\sum_{i=q,\bar{q}} e_i^2 x f_i(x,Q^2) \tag{4}$$

where f_i is the structure function for a quark of flavour i with electric charge e_i. The same basic structure holds also for the weak processes, but with other Q^2-dependent propagators, y-dependent helicity factors and flavour couplings. QCD corrections are included through the Q^2 dependence of the structure functions. QED radiative corrections, in particular photon bremsstrahlung off the incoming lepton, introduce further complications. These are not considered in the present paper, since they are normally corrected for in the experimental data.

2.2 Matrix Elements

The lowest order (QPM) partonic process $\gamma^* + q \to q$ is in first order QCD supplemented by gluon radiation and boson-gluon fusion, $\gamma^* + q \to q + g$ and $\gamma^* + g \to q + \bar{q}$, as shown in Fig. 2. (The virtual photon may here also symbolize a general electroweak exchange of W and γ/Z bosons.) The matrix elements [9] are, for each given x and Q^2, complicated functions of three (Lorentz invariant) variables. These variables correspond to the new degrees of freedom in terms of, e.g., the relative sharing of energy between the two scattered partons, the opening angle between them, and an azimuthal angle with respect to the scattered lepton direction. Although the azimuthal dependence can often be

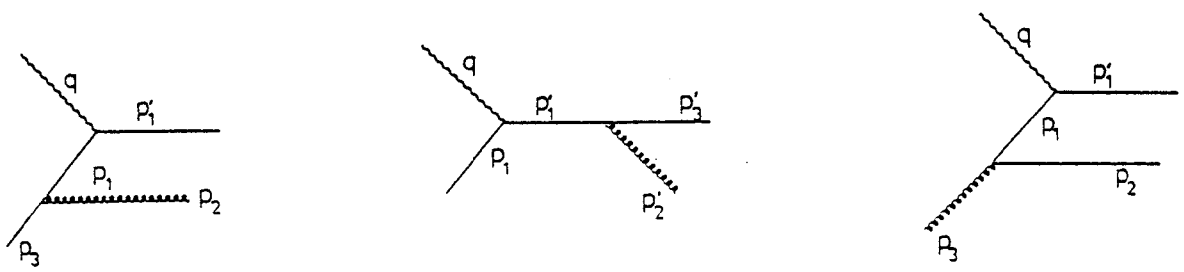

Figure 2: *The first order QCD processes, gluon radiation and boson-gluon fusion, giving the lowest order corrections to the basic process in Fig. 1.*

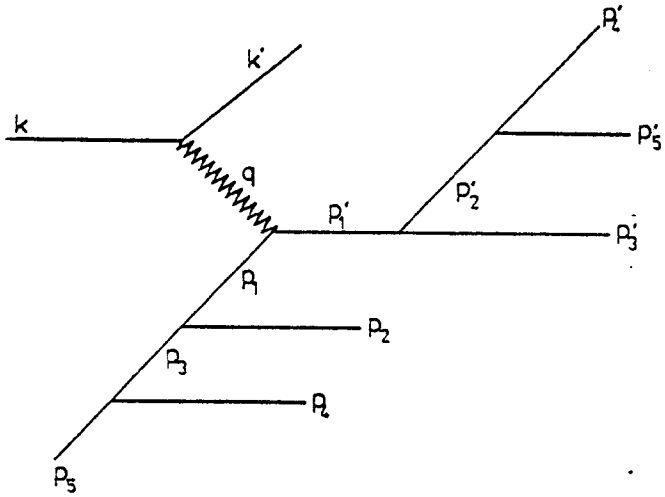

Figure 3: *Schematic drawing of the QCD branching processes in initial and final state radiation. (The lines with momenta p symbolize partons in general, i.e. quarks and gluons.)*

neglected to first approximation, it is included for completeness in our treatment. The matrix elements are divergent in the limit when the gluon energy or the opening angle vanishes (soft or collinear singularities). These divergences are partly cancelled by virtual corrections to the lowest order graph, and partly absorbed in the Q^2-dependent structure functions.

For convenient Monte Carlo simulation of events, it is necessary to impose a cutoff on the singular regions of the first order matrix elements. This can be done e.g. by requiring a minimum invariant mass m_{cut} between any pair of partons in the hadronic final state (with the target remnant system counted as one parton). From a physical point of view, it would be natural to assume m_{cut} independent of W. However, with increasing W the first order processes would then ultimately obtain a probability larger than unity. It is therefore necessary to allow for some variation in m_{cut} as a function of W (and x). The complete electroweak scattering cross-section, exact first order QCD matrix elements and target remnant treatment are implemented in a Monte Carlo event generator [10] which has been used for the results in this paper. The quark distribution functions given by EHLQ set I [11] have been used throughout, but we note that our results are not sensitively dependent on the specific structure function parametrization used.

2.3 Parton Showers

An alternative to matrix elements is provided by parton showers, schematically illustrated in Fig. 3. In a discussion of parton showers, it is necessary to distinguish between initial state showers, where the branches occur before the photon vertex, and final state showers, where they occur after the photon vertex. The separation of these two possible time orderings implies a neglect of the interference terms in Fig. 2, and is of course not gauge invariant. In the collinear regions, close to the incoming or outgoing parton directions, the correct results should still be obtained, while wide angle emission could be misrepresented. In e^+e^- physics this problem was possible to overcome, at least partially, by matching on to the lowest order matrix elements. Here it is considerably more difficult to perform the corresponding analysis.

If one may view a complete interaction at the hadronic side in a 'chronological' order, the initial state consists of a set of partons, close to mass-shell ($\approx$ 1 GeV), whereof one initiates a cascade. In each branch of this cascade, one of the daughters continues towards the hard interaction vertex with increasing spacelike virtuality, while the other one is on mass-shell or acquires a timelike virtuality (in which case it will develop a timelike shower of its own). The spacelike shower is therefore characterized by increasing Q^2, decreasing energies and increasing (average) opening angles. Once the incoming

spacelike quark has been struck by the boson, the outgoing quark is now timelike, or at least on mass-shell. This timelike quark starts to shower into daughters with decreasing off-shell masses. In the shower, the opening angles between daughters are decreasing, as are the daughter energies. The basic behaviour of initial and final state showers alike is regulated by the Altarelli-Parisi equations [12], but with important differences as to details, as will be discussed below.

In matrix element calculations all external legs are on mass-shell and, because of the inclusion of interference terms, it is not meaningful to ask what is the virtuality of intermediate partons. The situation is quite the opposite in parton shower algorithms, where the generation of spacelike or timelike masses is a central ingredient. This leads to complications in the definition of the Bjorken x variable, as follows, Fig. 3. From the kinematics of the lepton vertex, the Bjorken x is unambiguously defined as $x = Q^2/2P \cdot q$. It is also possible to define an $x' = p_1 \cdot q/P \cdot q$, i.e. (in the Breit frame, $q = (0; 0, 0, Q)$) the longitudinal momentum of the struck quark as a fraction of the momentum of the original proton. These two coincide for massless incoming and outgoing partons, since then

$$0 = p_1'^2 = (p_1 + q)^2 = p_1^2 + 2p_1 \cdot q + q^2 = x' 2P \cdot q - Q^2 \quad \Rightarrow \quad x' = \frac{Q^2}{2P \cdot q} = x \tag{5}$$

If the incoming parton has a spacelike virtuality $p_1^2 = -Q_1^2$ and/or the outgoing parton a timelike virtuality $p_1'^2 = m_1'^2$, this relation is changed to

$$\begin{aligned} m_1'^2 = p_1'^2 &= (p_1 + q)^2 = p_1^2 + 2p_1 \cdot q + q^2 = -Q_1^2 + x' 2P \cdot q - Q^2 \\ \Rightarrow \quad x' &= \frac{Q^2 + Q_1^2 + m_1'^2}{2P \cdot q} = x \left(1 + \frac{Q_1^2 + m_1'^2}{Q^2}\right). \end{aligned} \tag{6}$$

Serious mismatches may thus occur between x and x', in extreme cases even with $x' > 1$. Although kinematically possible, such situations would cause other problems in the model. A possible solution will be presented in the next section.

The usual interpretation of the structure function $f_i(x, Q^2)$ is that it gives the probability to find a parton with flavour i, taking a fraction x of the hadron energy or momentum, if the hadron is probed at the 'scale' Q^2. The exact choice of energy and momentum combination in the x definition is obviously irrelevant for massless partons (and negligible transverse momenta), but matters if partons are off mass-shell. Experimentally, structure functions are determined by measurements of the scattered lepton. In order to reproduce the correct differential cross-section, eq. (4), one is therefore obliged to use the Bjorken x definition, i.e. let the lepton vertex be unaffected by the evolution of parton showers. The alternative would have been to find a completely new set of structure functions, e.g. in terms of the x' defined above, based on an explicit model for the distribution of parton virtualities — a major task.

2.4 Spacelike Showers

The partons inside an incoming hadron may be viewed as undergoing a continuous process of branchings and recombinations. Each branching $a \to bc$ involves some relative transverse momentum between the partons b and c. In a language where four-momentum is conserved at each vertex, this implies that at least one of the b and c partons must have a spacelike virtuality. Since the partons are virtual, a cascade only lives a finite time before reassembling, with the most off-shell partons living the shortest time. In a hard scattering, the larger the momentum transfer scale is, the smaller are the distances probed in the hadron, and the softer is the parton composition observed. This is expressed by the Altarelli-Parisi evolution equations [12]

$$\frac{df_b(x,t)}{dt} = \frac{\alpha_s(t)}{2\pi} \sum_a \int \frac{dx'}{x'} f_a(x',t) P_{a\to bc}\left(\frac{x}{x'}\right) \tag{7}$$

Here the $f_i(x,t)$ are the usual structure functions and t is shorthand for $ln(Q^2/\Lambda^2)$. Thus the first order strong coupling constant is

$$\alpha_s(Q^2) = \frac{12\pi}{(33-2n_f)t} = \alpha_s(t) \tag{8}$$

where n_f is the number of flavours. Finally, the Altarelli-Parisi splitting kernels $P_{a\to bc}(z)$ are given by

$$P_{q\to qg}(z) = \frac{4}{3}\frac{1+z^2}{1-z}\ ;\ P_{g\to gg}(z) = 6\frac{(1-z(1-z))^2}{z(1-z)}\ ;\ P_{g\to q\bar{q}}(z) = \frac{1}{2}(z^2+(1-z)^2) \tag{9}$$

The presence of a hard interaction reduces a cascade to a single sequence of branchings $a \to bc$, where a and b are on the main chain of increasing spacelike virtuality, while $m_c^2 \geq 0$. A 'forwards' evolution scheme, where the evolution of the shower is traced from some initial Q_0^2 up to the hard scale Q^2, is awkward technically, since it is then difficult to match up the spacelike shower with the hard interaction cross-section, and since the kinematics can not be constructed until it is known which branch is the one struck by the virtual photon. Instead a 'backwards' evolution scheme has been developed [13,14], where the spacelike parton shower is reconstructed from the hard interaction backwards, i.e. in falling Q^2 sequence, as follows.

The Altarelli-Parisi equations express that, during a small increase dt there is a probability for a parton a with momentum fraction x' to become resolved into a parton b at $x = zx'$ and a parton c at $x' - x = (1-z)x'$. Correspondingly, during a decrease dt a parton b may be 'unresolved' into a parton a. The conditional probability dP_b for this to happen is given by df_b/f_b which, using eq. (7), becomes

$$dP_b = \frac{df_b(x,t)}{f_b(x,t)} = |dt|\frac{\alpha_s(t)}{2\pi}\sum_a \frac{dx'}{x'}\frac{f_a(x',t)}{f_b(x,t)}P_{a\to bc}(\frac{x}{x'}). \tag{10}$$

Summing up the cumulative effect of many small changes dt, the probability for no radiation exponentiates. Therefore one may define a 'Sudakov' form factor

$$S_b(x,t_{max},t) = exp\left\{-\int_t^{t_{max}} dt'\,\frac{\alpha_s(t')}{2\pi}\sum_a\int dz P_{a\to bc}(z)\frac{x' f_a(x',t')}{x f_b(x,t')}\right\} \tag{11}$$

giving the probability that a parton b remains at x from t_{max} to $t < t_{max}$.

A knowledge of S_b is enough to trace the evolution backwards. The virtuality (the t value) of parton b is essentially obtained directly from eq. (11); a number of technical complications are described in [13]. For a given t of a branching, the relative probabilities for different allowed branchings $a \to bc$ are given by the z integrals in the sum in eq. (11). Finally, with t and a known, the probability distribution in the splitting variable $z = x/x' = x_b/x_a$ is given by the z integrand in eq. (11). With parton b given, the process may now be repeated for parton a to find its virtuality and origin, and so on until a virtuality is chosen below some small cutoff scale Q_0^2, which typically is taken to be 1 GeV^2.

In order to explicitly construct the four-momenta of the partons in the showers, and in particular the transverse momenta at branchings, a precise z definition is required. In the limit where virtualities are small compared to energies, and where transverse momenta are also small, all definitions of z should only differ by terms of order Q^2/s. Differences occur in general, however, and a given definition may be chosen for technical simplicity. The choice used in this program (here written for the branching closest to the hard interaction) is [6]

$$z_1 = \frac{p_1\cdot q - Q_1^2}{p_3\cdot q - Q_3^2} = \frac{p_1\cdot(p_1+q)}{p_3\cdot(p_3+q)} \tag{12}$$

(Also another, rather different z choice has been studied, but physics results were fairly similar.)

With the kinematics as defined so far, the longitudinal momentum constructed for the on mass-shell shower initiating parton n will disagree with the one obtained from interpreting $x_n = x/\prod z_j$ as the fraction of incoming proton momentum. There are two sources for this mismatch. One is the discrepancy between $p_1 \cdot q/P \cdot q$ noted in eq. (6), the other comes from the z definition introduced in eq. (12). The most straightforward solution, which is also the one adopted, is to redefine the first x used in the evolution according to

$$x_1' = x_1(1 + \frac{m_1'^2 - Q_1^2}{Q^2}). \tag{13}$$

This exactly compensates for the errors above.

In the section above, Q^2 has been used to denote a particle virtuality or an argument in α_s and in structure functions. It is in the nature of perturbative QCD that the definition of Q^2 in α_s is not unique. In particular, loop calculations tend to indicate that the proper argument for α_s is not Q^2 but $p_T^2 \approx (1-z)Q^2$ [15]. Such corrections can be taken into account if desired, but are not of crucial importance for the results reported here.

2.5 Timelike Showers

The timelike or final state showers appear for the quark scattered off the current q and, less importantly, for the side branches of the initial state cascade. The following discussion is concentrated on the former case, with the latter obtained by a fairly straightforward generalization. In order to describe the timelike shower evolution, the model presented in [16] will be used. This model is originally developed for e^+e^- annihilation events, where there are two cascading partons in the final state rather than one; this necessitates some modifications.

For the first branching $1' \to 2' + 3'$ in a timelike shower, a splitting variable z_1' is defined by

$$z_1' = \frac{p_0 \cdot p_2'}{p_0 \cdot p_1'}, \tag{14}$$

where $p_0 = P + q$. In the hadronic rest frame $p_0 = (W; 0, 0, 0)$, and z_1' reduces to $z_1' = E_2'/E_1'$, i.e. energy fractions. The p_0 is kept as 'reference vector' in subsequent branchings. Because of the choice of frame, the maximum kinematically allowed mass of the shower is $(m_1')_{max} = E_1' = W/2$.

The evolution of a parton in the cascade is once again given by a Sudakov form factor, which expresses the probability that a parton a does not branch between some initial maximum mass-square m^2 and a minimum value m_0^2

$$S_a(m^2) = exp\left\{-\int_{m_0^2}^{m^2} \frac{dm'^2}{m'^2} \int dz \frac{\alpha_s}{2\pi} P_{a\to bc}(z)\right\}. \tag{15}$$

The Altarelli-Parisi kernels, $P_{a\to bc}(z)$, are identical with those given in eq. (9). The Sudakov form factor can be used to find the mass of the decaying parton, the z value in its branching and the flavours of the daughters. These daughters may be evolved in their turn, and so on. The shower is traced down to some minimum cutoff virtuality m_0^2 (here taken to be 1 GeV^2).

A number of special features of timelike showers are known and included. One is coherence among soft gluons, which leads to angular ordering: the opening angles of branches are constrained to decrease monotonically as the masses are evolved downwards [17]. Another aspect is the freedom to use different scales as argument in α_s, as in the spacelike case. Studies of coherence effects [18] suggest that the $p_T^2 \approx z(1-z)m^2$ of the daughters is preferable to use as an argument.

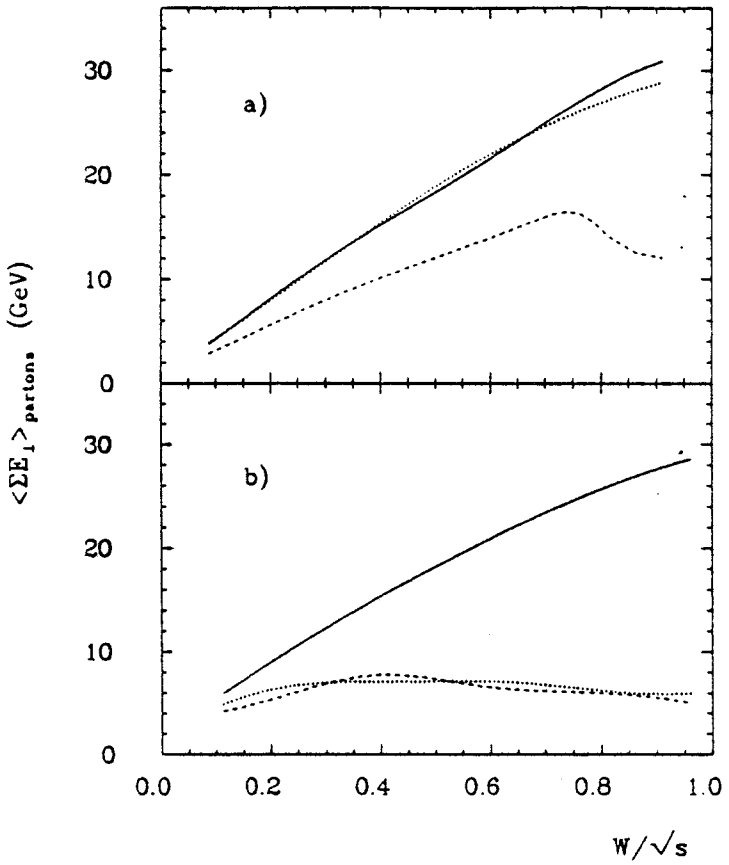

Figure 4: *Average summed transverse energy of partons,* $< \sum E_\perp >$, *as a function of* $W/\sqrt{s}$ *at HERA energy for a)* $Q^2 = 10^4$ GeV^2 $(Q^2/s = 0.1)$ *and b)* $Q^2 = 100$ GeV^2 $(Q^2/s = 0.001)$. *Parton shower (PS) with maximum virtuality* W^2 *(full line), with* Q^2 *(dotted line) and for first order matrix elements (ME) (dashed line).*

The evolution of spacelike and of timelike parton showers have been considered separately above. In order to complete the description of this scheme, the two components have to be put together, as follows. With x and Q^2 chosen from the differential electroweak cross-section it is straightforward to construct q, p_1 and p_1', put along the z axis in the hadronic CM frame, with p_1 and p_1' on mass-shell. The timelike quark leg p_1' is evolved and acquires a mass m_1'. While the energy is preserved in the process, the longitudinal momentum is not. Before considering momentum conservation, the spacelike leg is evolved, to give $p_1^2 = -Q_1^2$, and the four-momentum p_1 is constructed such that $m_1'^2$ is taken into account in the equations in section 2.4. At the end of the spacelike cascade evolution, an on-mass-shell initiator parton is constructed, with momentum p_{init}. By virtue of the rotations and boosts performed in connection with each branching, p_{init} is along the z axis, as is the unchanged q vector, while p_1 now has a transverse momentum. The four-momentum $p_1' = p_1 + q$ of the timelike shower initiator is now known, and the timelike shower already constructed can be boosted and rotated to give agreement. After the hadron remnant has been added, the system can be boosted from the hadronic CM frame to any desired frame.

It is ambiguous what sets the scale for the maximum virtuality in the shower. The natural alternatives here are Q^2 and W^2 (or more generally a function of these two variables). A scheme for matching on to the exact first order matrix elements for deep inelastic scattering, which could resolve this, is in progress [19]. A potential problem of double counting of emission is present when bremsstrahlung from the spacelike and timelike leg is added incoherently. For hard emission it becomes important to take into account constraints from structure functions on the first timelike branching. Kinematical

constraints relating the timelike and spacelike evolution must be solved before a consistent matching procedure on to the matrix element can be performed. Lacking a working model of this kind we note that, although Q^2 is the fundamental parameter in the matrix elements, the x-dependent factors make the basic transverse momentum properties depend mainly on W^2 (for not too small x) [9]. One way to study the effects of the different possibilities is shown in Fig. 4, where average summed $E_\perp$ of partons is plotted as a function of W for different fixed Q^2 values. For reasonably large Q^2, PS with either Q^2 or W^2 (properly speaking $W^2/4$ [6]) as maximum virtuality then agree with the ME result (considering that the ME approach does not include the soft gluon region covered by the PS one), whereas for $Q^2 \ll W^2$ (x small) the use of Q^2 as scale would seem preferrable, if the ME results are used as guideline. This is only half of the story, however: even with $Q^2 \ll W^2$ the ME approach does contain a tail of high-$p_\perp$ jets, which is entirely absent with an abrupt PS cutoff at virtuality Q^2. In a Monte Carlo approach, it is therefore preferable to use W^2 as scale, but then apply rejection techniques to match on to the hard emission matrix element results. Based on these considerations we choose to use W^2 for the maximum virtuality, but note that our results are not very sensitive to this choice since we impose cuts that avoid the problematic low-x region. In the spirit of the leading log approximation, one would then expect soft and collinear gluon emission to be well described by parton showers, whereas the amount of hard radiation is somewhat uncertain.

2.6 Fragmentation

Once the parton configuration of a leptoproduction event has been specified, by matrix elements or parton showers, the fragmentation of these partons can be described, e.g., by the Lund string fragmentation model [1,20]. In the simplest case, valence quark scattering without gluon emission, a string is stretched between the scattered quark and the remnant diquark. For more complicated events there may be one or more strings, each corresponding to a colour singlet subsystem. Each string is stretched between a quark end and an antiquark or diquark one, with gluons appearing as energy and momentum carrying kinks on these strings. In first order matrix elements and leading log shower evolution alike, the way the strings should be stretched between the scattered partons (i.e. their colour ordering) is unambiguous; problems would arise with exact second order matrix elements, however.

The treatment of the hadron remnant system is not unique, except possibly when a valence quark is 'kicked out' of the incoming hadron, leaving behind a diquark system. For processes which give a more complex remnant, phenomenological recipies must be employed [21]. In the boson-gluon fusion process (or a parton shower initiated by a gluon), the colour octet qqq-remnant is subdivided into a colour triplet quark and an antitriplet diquark, sharing the available energy according to an assumed distribution, and connected by two independent strings to the produced antiquark and quark, respectively. Correspondingly, if a sea antiquark (quark) is kicked out of a nucleon, the remaining $qqqq$ ($qqq\bar{q}$) system, which contains the partner quark (antiquark) to the struck one, is divided into a baryon plus a quark (a meson plus a diquark); the latter is connected with a string to the struck quark. Sensible recipes are here included in the Monte Carlo descriptions.

3 Event Properties at HERA Energies

While the QPM fails to describe event properties already at present energies, either the ME or the PS option give a reasonable description of the data [22,7]. Some $p_\perp$ quantities do, however, require the inclusion of soft gluon effects in the ME approach, i.e. a step towards the PS one. At HERA, with $\sqrt{s}$ = 314 GeV, the ME and PS results will differ substantially in some aspects. However, since the

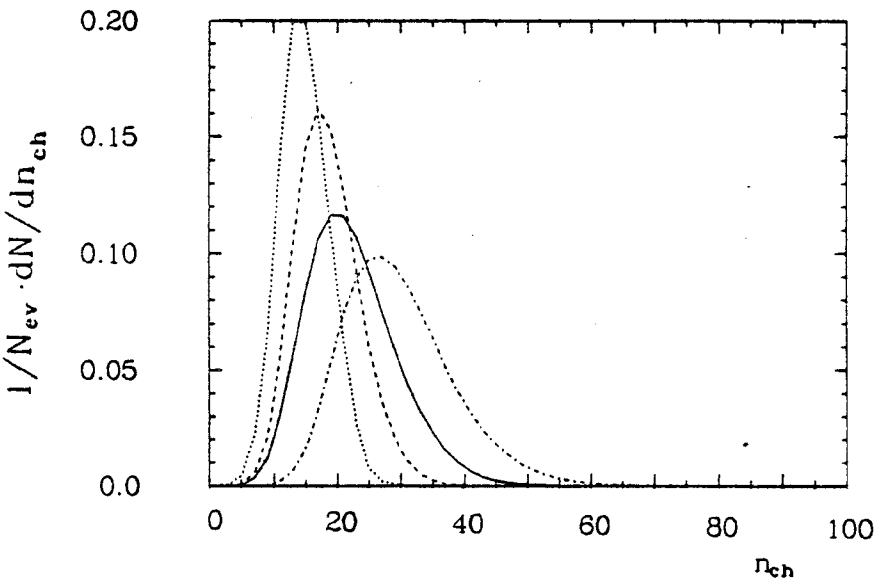

Figure 5: *Charged multiplicity distributions for HERA neutral current events with W = 163 GeV (x = 0.1, y = 0.3). QPM dotted, ME dashed, PS full, e^+e^- events of same energy dash-dotted.*

main difference between ME and PS is the lack of extra soft jets in the former description, the overall event shapes should still show a large similarity.

For the following predictions of HERA event properties, we normally use neutral current event samples (with full γ/Z^0 structure) defined by lower cuts in Q^2 and W^2, in order to concentrate on the new and interesting region. The cuts Q^2, $W^2 > 10^3$ GeV^2 amount to having these variables larger than $\approx 1\%$ of the maximum possible, and the resulting cross-section in the standard model is 215 *pb*, leading to a useful event sample with realistic luminosities. For some observables the influence of varying kinematics is not desirable, since that washes out the interesting effects. In such cases we fix the kinematics at $x = 0.1$, $y = 0.3$, i.e. $Q^2 = 2950$ GeV^2 and $W = 163$ GeV, which are approximately the mean values in the region defined above. Since our objective is to study the hadronic final state, the scattered lepton is never included in the following studies.

The charged multiplicity distributions are shown in Fig. 5 for events with fixed kinematics. Note that not only the mean values $< n_{ch} >$ are increased when going from QPM to ME to PS events, but even more so the width, i.e. the distributions become increasingly non-Poissonian. Already the QPM distribution is wider than a Poissonian, as a consequence of the hadron remnant. e^+e^- events, simulated with the same final state parton shower algorithm and at the same energies, show even larger multiplicities and fluctuations.

The importance of the baryon produced in the target region has already been noted [3]. This importance is not an effect that disappears with increasing energy, see Fig. 6 for the z-weighted x_F-spectrum of charged particles ($z = 2E/W$, $x_F = 2p_z/W$ in the hadronic CM frame). The rapidity distributions in the hadronic CM frame, Fig. 7, not only show the unequal fragmentation regions but also that QCD radiation predominantly occurs in the forward region (also the $< p_\perp >$ values are significantly larger there).

In Fig. 8 a corresponding distribution is studied on the parton level for the parton shower model. The separation into a spacelike and a timelike shower is not gauge invariant, but for practical purposes one may accept it as a first approximation. In Fig. 8a is plotted the parton rapidity distributions in the hadronic CM frame, separately for the timelike and the spacelike showers. The two cascades are fairly well separated, i.e. to be found in the forward and in the backward hemisphere, respectively. The

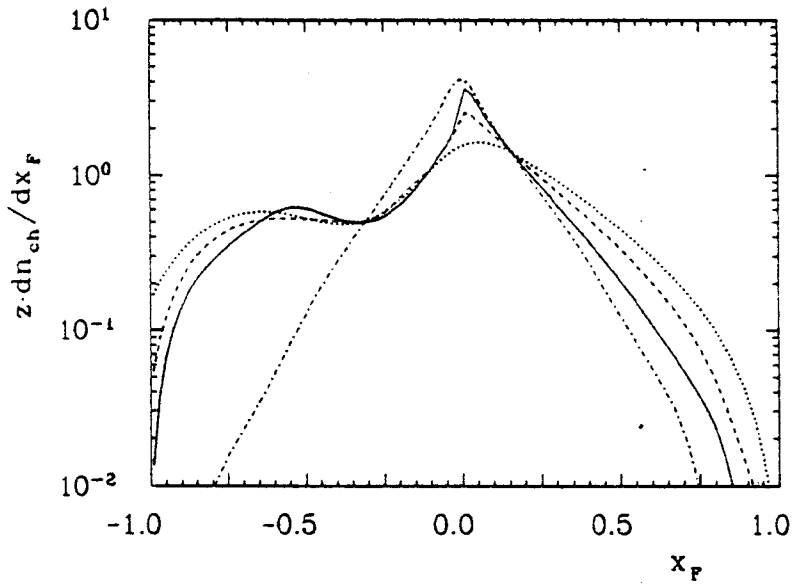

Figure 6: *Energy-weighted distribution of scaled longitudinal momenta, $z \cdot dn_{ch}/dx_F$, for charged particles in the hadronic CM frame of HERA events with Q^2, $W^2 > 10^3$ GeV^2 ($x_F > 0$ for the current jet and < 0 for the beam one). QPM dotted, ME dashed, PS full, e^+e^- events of same energy dash-dotted.*

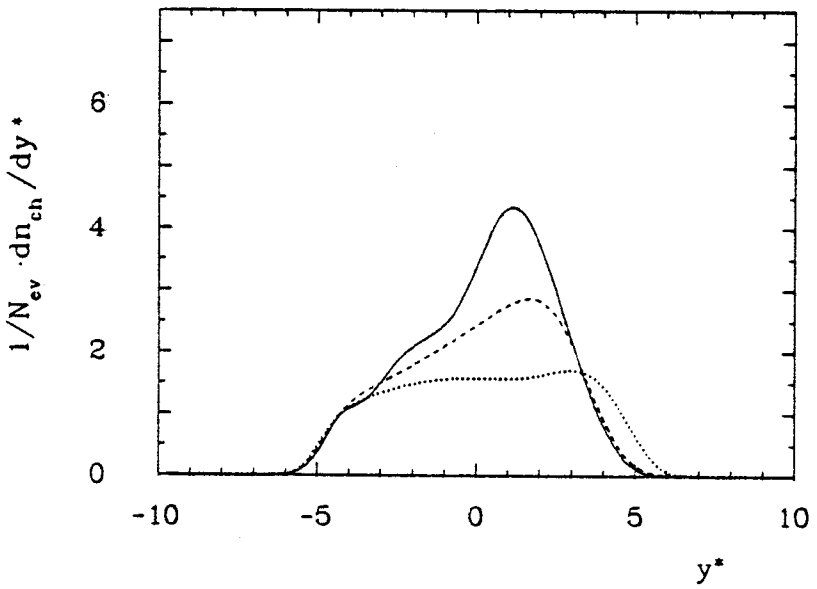

Figure 7: *Charged particle rapidity distribution, $1/N_{ev} \cdot dn_{ch}/dy^*$, in the hadronic CM frame. HERA events with Q^2, $W^2 > 10^3$ GeV^2. QPM dotted, ME dashed, PS full.*

number of partons is obviously not an infrared safe quantity; a better representation is provided by the $p_\perp$-weighted rapidity distribution, Fig. 8b. The spacelike shower is here shown to be concentrated more towards the central rapidity region than the timelike one. This is simply because a large part of the hadron, the remnant, does not take part in the interaction, and ends up far out in the backwards hemisphere with negligible transverse momentum.

From Fig. 8b it is also obvious that the timelike shower generates more transverse momentum than does the spacelike one. One must remember, however, that the transverse momentum of partons emitted in the spacelike cascade is balanced by the struck quark, so that the timelike shower is

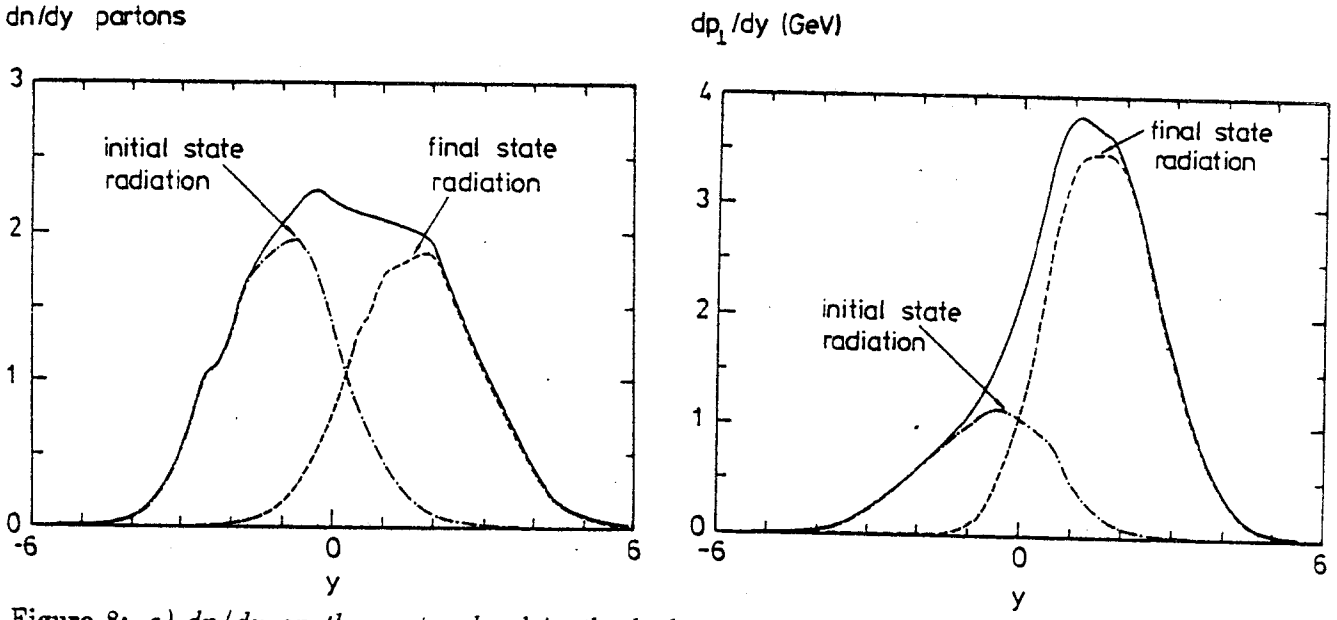

Figure 8: *a) dn/dy on the parton level in the hadronic CM frame, plotted separately for final state partons (dotted line), initial state partons (dash-dotted) as well as the sum of the two (full). HERA events with $x > 0.1$ and $y > 0.1$.*
b) $dp_\perp/dy$ with notation as in a).

developed along a direction tilted away from $p_\perp = 0$ already from the start. This contributes to the asymmetry, but it is also true (in the model) that the average spacelike virtuality of the struck quark is smaller than the average timelike virtuality of the quark directly after the hard scattering [6].

In order to characterize event shapes, Table 1 gives the mean values of $< S_{lin} >, < A_{lin} >$ (linear sphericity and aplanarity measures) and $< n_{jet} >$ (using LUSPHE and LUCLUS in [20]) for charged particles. Here $< S_{lin} >$ gauges the general level of non-twojetness, while $< A_{lin} >$ measures the activity out of the event plane, and thus only receives parton level contributions from four-jets and onwards. While the ME and PS show a similar behaviour in the former quantity, PS are bound to give a much larger $< A_{lin} >$ at HERA energies. The number of reconstructed jets tells a similar story as $< A_{lin} >$ does. Again note the strong forward-backward asymmetry in jet activity.

Table 1

Event shape properties of charged particles in the hadronic CM frame for HERA with Q^2, $W^2 > 10^3$ GeV^2. Mean values of linear sphericity and aplanarity, number of reconstruced jets and the difference between number of jets in the forward (current) and backward hemisphere.

	$< S_{lin} >$	$< A_{lin} >$	$< n_{jet} >$	asymmetry
QPM	0.033	0.010	1.98	0.02
ME	0.075	0.016	2.40	0.26
PS	0.104	0.026	2.79	0.47
e^+e^-	0.150	0.035	3.18	-

While the hadronic CM frame is convenient for theoretical event studies, the boost from the lab frame to the hadronic CM frame does presuppose a knowledge of the event kinematics as well as hadron masses. Therefore studies in the lab frame have a certain interest. In terms of rapidity distributions,

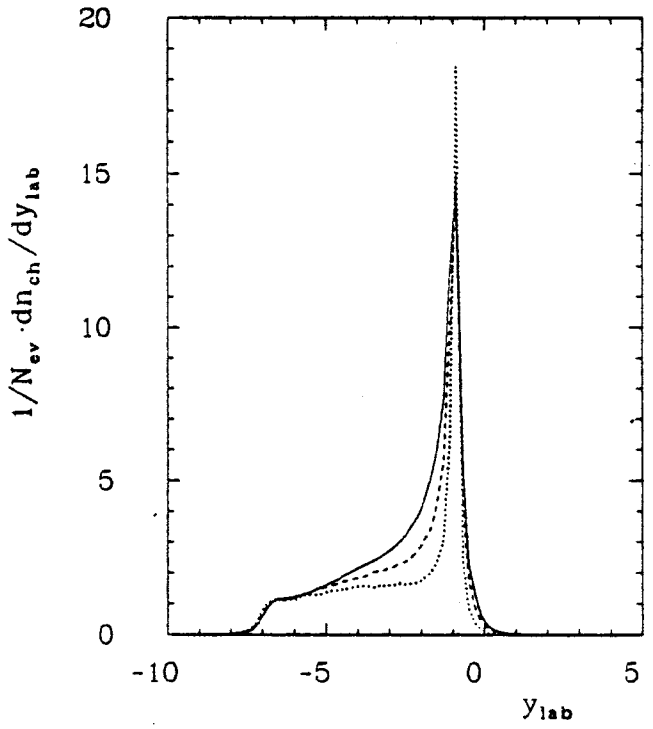

Figure 9: *Charged particle rapidity distribution,* $1/N_{ev} \cdot dn_{ch}/dy$, *in the lab frame for HERA events with* $x = 0.1$, $y = 0.3$. *QPM dotted, ME dashed, PS full.*

the beam jet looks the same, apart from an overall shift by $ln[2(1-x)|P|/W]$. The current jet is now fairly well compressed around the naive direction of the scattered quark, again with QPM giving the narrowest and PS the broadest distribution, Fig. 9. This difference is also visible in the energy flow in the event plane, Fig. 10. (It should be noted, that even in the QPM model the energy and angle of the current jets are not exactly those expected from naive kinematics, due to the primordial $k_\perp$.)

When different kinematical configurations are averaged over, the sharp dn/dy peak is smeared out, and what remains is a general increase in the 'forward' region, where the current jets are to be found. In the QPM the resulting 'forward-backward' asymmetry is almost entirely kinematical in origin, whereas the ME and PS contain a further enhancement of the forward multiplicity from extra jet activity.

A broadening of jet width in azimuthal angle (around the beam axis), i.e. $dn/d\phi$, is also visible in a comparison between QPM, ME and PS. However, this broadening does not lead to significant changes 180° away from the scattered quark direction ($\lesssim$ factor 2). In particular, the isolation of the scattered electron is usually not worse because of the additional gluon radiation in PS compared to the ME case. A tiny class of events does appear, however, where the electron overlaps with a jet, which may make the electron energy measurement more difficult.

For an explicit jet reconstruction in the lab frame, it is convenient to use the variables pseudo-rapidity (η), azimuthal angle (ϕ) and transverse energy ($E_\perp$) in a jet finding algorithm of the generic UA1 type (LUCELL in [20]). In the algorithm, the transverse energy in all cells within a distance $\omega = \sqrt{\Delta\eta^2 + \Delta\phi^2} < \omega_{max}$ around an 'initiator' cell are summed up, and if the $\Sigma E_\perp > E_{\perp min}$ for some threshold transverse jet energy $E_{\perp min}$, these cells together define one jet. In the following, typically $E_{\perp min} = 5$ GeV and $\omega_{max} = 0.5$ will be used. It should be pointed out that this kind of procedure is very convenient and natural in events where the current jet is reasonably central, but it may need to be modified for a search of very forward current jets. A separate and more complete study of jet finding

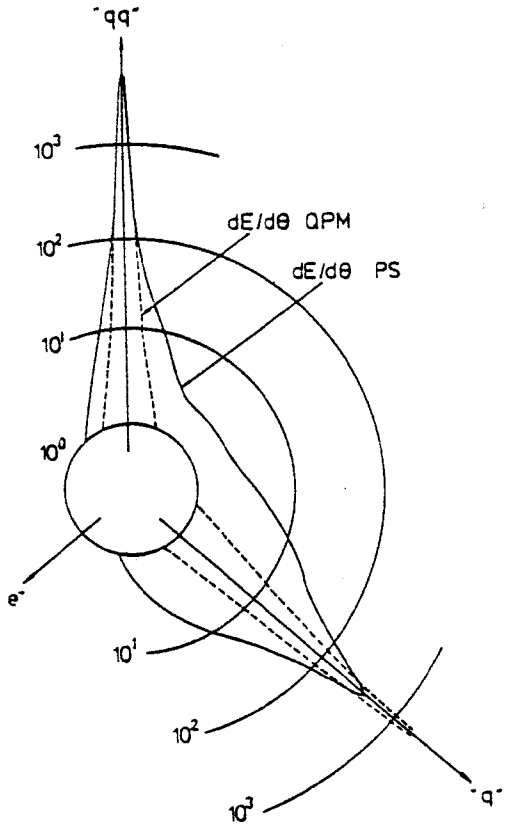

Figure 10: *The energy flow in the event plane, $dE/d\theta$ plotted for HERA events with $x = 0.2$ and $y = 0.5$. The full line is for the parton shower model, while the dashed one is for the quark parton model. Directions of the scattered electron, scattered parton ('q') and target remnant ('qq') as given by naive parton model kinematics.*

at HERA, considering this problem and also taking experimental resolution into account, is reported in [25]. (There is also no built-in symmetry between finding jets resulting from initial and from final state radiation; for that, analyses in the hadronic CM frame are preferable.) For the following simple jet study to illustrate the most important effects, we neglect these problems and have therefore chosen the fixed kinematics configuration mentioned above which means a naive current jet at 44° from the proton beam direction.

Resulting jet multiplicity distributions are shown in Fig. 11. The probability that more than one jet is found in the QPM case is exceedingly small, while several jets are found frequently with ME and PS. One jet is here usually fairly hard, and is to be found close to the naive current jet direction, whereas the softer jets are predominantly found shifted towards the beam jet direction, but still at fairly central rapidities. This is shown by the pseudorapidity distribution $dn_{jet}/d\eta$ for the reconstructed jet directions in Fig. 12. Note that, while a very few jets are to be found closer to the target jet region with ME or PS than with QPM, most of the increased jet activity from higher order QCD is to be found in the same region as the current jets. This observation, also true in an event sample with varying kinematics, is not entirely trivial, since the kinematically allowed η range of emission is larger for the 'extra' lower-energy jets. The number of jets found is obviously a function of the algorithm parameters. In Fig. 13 is shown the effects of varying ω_{max} from 0.1 to 2, while keeping $E_{\perp min} = 5$ GeV fixed. Again, parton shower events are seen to have a richer subjet structure than matrix element ones. For very small ω_{max}, the algorithm becomes sensitive to the 'calorimeter' granularity and is therefore less reliable.

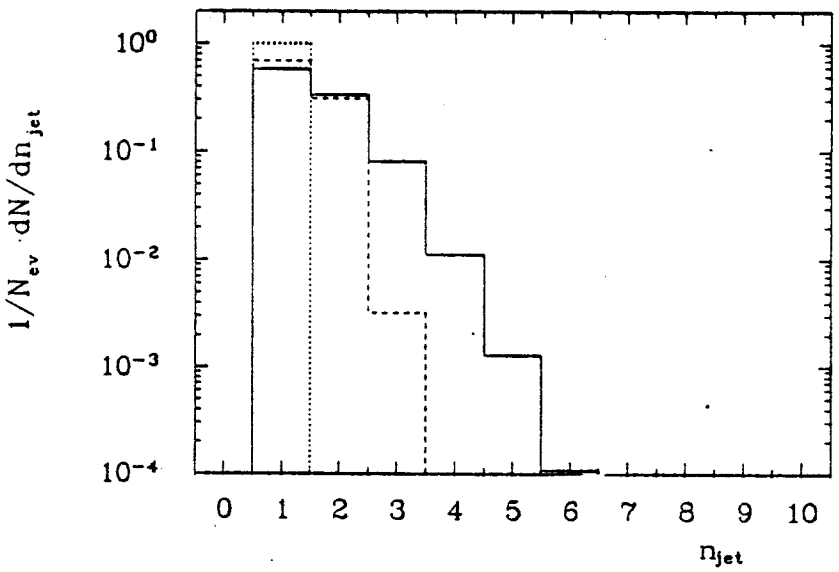

Figure 11: *Multiplicity distribution of reconstructed jets for HERA events with* $x = 0.1$, $y = 0.3$. *QPM dotted, ME dashed, PS full.*

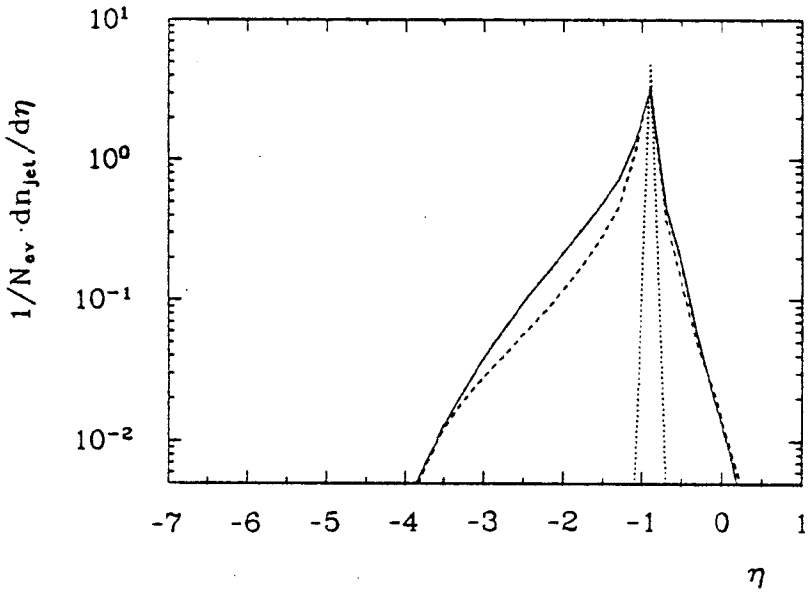

Figure 12: *Pseudorapidity distribution* $1/N_{ev} \cdot dn_{jet}/d\eta$ *of reconstructed jets for HERA events with* $x = 0.1$, $y = 0.3$. *QPM dotted, ME dashed, PS full.*

4 Summary

It has been known for a long time that the quark parton model description fails to account for a number of observed properties of leptoproduction events. A generally good description has been obtained with an approach based on first order matrix elements. There have been a few distributions, notably those for transverse momentum compensation, where agreement has not been entirely satisfactory. In order to understand these, soft gluon effects have been invoked and, with a simple soft gluon simulation scheme, good agreement with the data has indeed been obtained. In [7] we have shown that a parton shower approach is equally successful (except for a too low $< p_\perp^2 >$ at large x_F), and this without the need for an artificial separation into hard and soft radiation. Good agreement is only obtained if the

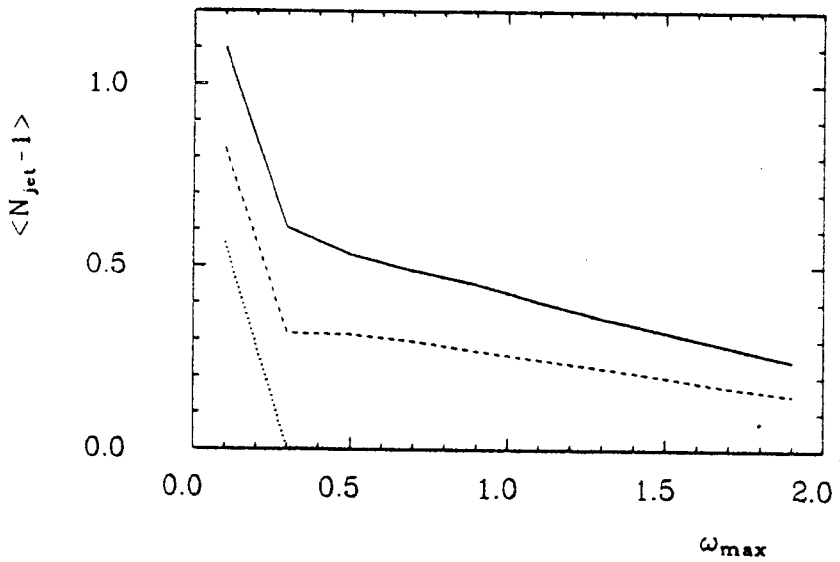

Figure 13: *Average number of reconstructed jets (subtracting one to account for the trivial current jet) as a function of jet cone opening angle ω_{max} in the jet finding algorithm, applied to HERA events with $x = 0.1$, $y = 0.3$. QPM dotted, ME dashed, PS full.*

parton shower cutoffs are chosen fairly small, e.g. $m_0 = Q_0 = 1$ GeV, in agreement with experience from e^+e^- annihilation.

Further studies and developments of the parton shower alternative are certainly necessary. In particular, one needs to address seriously the question of phasing together the first order matrix elements, which should be more accurate for hard QCD emission, with the parton shower approach. It is also interesting to note that other parton shower programs now start to become available for leptoproduction [26], which should make possible fruitful comparisons.

At HERA energies, results obtained with the quark parton model are entirely misleading, since QCD effects are very important for the structure of the hadronic system. For overall event properties, the approach based on first order QCD matrix elements and that of parton cascades show more agreement than might have been expected. Nonetheless, the higher order QCD effects included in parton showers give noticeable effects by making the events more 'smeared': they have larger multiplicity, broader current and target jets, more signs of multijet structure, etc. A limitation of the matrix element approach here is that a fairly large cutoff is required to avoid the divergences, and thus keep the total probability for first order QCD processes below unity. Despite the uncertainties present in the formulation of the parton shower alternative, it is therefore likely that the picture obtained here is also the more realistic one.

References

[1] B. Andersson, G. Gustafson, G. Ingelman, T. Sjöstrand, Phys. Rep. 97 (1983) 31

[2] B. Andersson, G. Gustafson, G. Ingelman, T. Sjöstrand, Z. Physik C9 (1981) 233

[3] G. Ingelman, B. Andersson, G. Gustafson, T. Sjöstrand, Nucl. Phys. B206 (1982) 239

[4] EMC Collaboration, J. J. Aubert et al., Phys. Lett. 95B (1980) 306, ibid. 100B (1981) 433

[5] T. Sjöstrand, Z. Physik C26 (1984) 93
JADE Collaboration, W. Bartel et al., Z. Physik C25 (1984) 231, ibid. C33 (1986) 23
Mark II Collaboration, A. Petersen et al., Phys.Rev.Lett.55 (1985) 1954, Phys.Rev.D37 (1988) 1
S. Bethke, Heidelberg Habilitation thesis, LBL 50-208 (1987)
T. Takahashi, Tokyo Ph.D. thesis, UT-HE-87/2 (1987)

[6] M. Bengtsson, T. Sjöstrand, Z. Phys. C37 (1988) 465

[7] M. Bengtsson, G. Ingelman, T. Sjöstrand, Nucl. Phys. B301 (1988) 554

[8] M. Bengtsson, G. Ingelman, B. Naroska, these proceedings.

[9] G. Altarelli, G. Martinelli, Phys. Lett. 76B (1978) 89
A. Méndez, Nucl. Phys. B145 (1978) 199
R. Peccei, R. Rückl, Nucl. Phys. B162 (1980) 125
Ch. Rumpf, G. Kramer, J. Willrodt, Z. Phys. C7 (1981) 337

[10] G. Ingelman, 'The Lund Monte Carlo for deep inelastic lepton-nucleon scattering — LEPTO version 5.2', DESY preprint in preparation.

[11] E. Eichten, I. Hinchliffe, K. Lane, C. Quigg, Rev. Mod. Phys. 56 (1984) 579, ibid. 58 (1986) 1047

[12] G. Altarelli, G. Parisi, Nucl. Phys. B126 (1977) 298

[13] M. Bengtsson, T. Sjöstrand, M. van Zijl, Z. Physik C32 (1986) 67

[14] H.-U. Bengtsson, T. Sjöstrand, Computer Phys. Comm. 46 (1987) 43

[15] A. Bassetto, M. Ciafaloni, G. Marchesini, Phys. Rep. 100 (1983) 201

[16] M. Bengtsson, T. Sjöstrand, Nucl. Phys. B289 (1987) 810

[17] A. H. Mueller, Phys. Lett. 104B (1981) 161
B. I. Ermolaev, V. S. Fadin, JETP Lett. 33 (1981) 269
G. Marchesini, B.R. Webber, Nucl. Phys. B238 (1984) 1

[18] D. Amati, A. Bassetto, M. Ciafaloni, G. Marchesini, G. Veneziano, Nucl. Phys. B173 (1980) 429
G. Curci, W. Furmanski, R. Petronzio, Nucl. Phys. B175 (1980) 27

[19] M. Bengtsson, Aachen preprint in preparation

[20] T. Sjöstrand, M. Bengtsson, Computer Phys. Comm. 43 (1987) 367
T. Sjöstrand, Computer Phys. Comm. 39 (1986) 347

[21] B. Andersson, G. Gustafson, G. Ingelman, T. Sjöstrand, Z. Physik C13 (1982) 361

[22] EMC Collaboration, M. Arneodo et al., Z. Physik C36 (1987) 527

[23] C. Basham, L. Brown, S. Ellis, S. Love, Phys. Rev. Lett. 41 (1978) 1585

[24] JADE Collaboration, W. Bartel et al., Z. Physik C25 (1984) 231

[25] P. Burrows, G. Ingelman, E. Ros, DESY 87-167 and these proceedings

[26] H. R. Wilson, Cavendish-HEP-87/10, Cavendish-HEP-88/2
G. Marchesini, B.R. Webber, Cavendish-HEP-87/8 and UPRF-87-212
K. Kato, T. Munehisa, KUDP-88/01 and YAMANASHI-88-1
G. Gustafson, U. Pettersson, private communication